TRANSVERSE INJECTION OF A PLANE REACTING JET INTO COMPRESSIBLE TURBULENT CHANNEL FLOW

Christoph Schaupp, Rainer Friedrich
Lehrstuhl für Aerodynamik und Strömungsmechanik
Technische Universität München
Boltzmannstr. 15, D-85748 Garching
c_schaupp@gmx.de, r.friedrich@lrz.tum.de

Holger Foysi
Aerodynamisches Institut
RWTH Aachen
Wüllnerstr. 5a, D-52062 Aachen
h.foysi@aia.rwth-aachen.de

ABSTRACT

A semi-implicit large-eddy simulation technique is used to predict transport and infinitely fast reaction processes of an H_2/N_2-jet injected through a narrow spanwise slot into a subsonic turbulent air flow between isothermal channel walls. The LES technique is based on approximate deconvolution and explicit modelling of the filtered heat release term. Spatial derivatives are computed using sixth order accurate central compact schemes. An explicit fourth-order Runge-Kutta algorithm serves for time-integration. Turbulent inflow conditions are generated by a separate LES of fully developed channel flow and are introduced well upstream of the injection station using characteristic boundary conditions. The complex transport processes in the vicinity of the injection region are highlighted by instantaneous and statistically averaged flow quantities.

INTRODUCTION

Transverse injection of fuel into compressible turbulent flow is a key feature of ramjet and scramjet technology. In most combustion chamber designs gaseous fuel is injected into the air stream at angles smaller than 90 degrees to the wall from ports in the duct wall or from pylons extending into the duct. Irrespective of the injection angle, the resulting flow, the mixing and reaction processes are very complex and not sufficiently understood. There is extensive previous work on incompressible jets in crossflow. Margason (1993) provides an overview of numerical and experimental investigations from 1932-1993. More recent DNS and LES studies are due to Muppidi & Mahesh (2007), Jones and Wille (1996), Wegner et al. (2004), Denev et al.(2009) and Renze et al. (2008), who investigated film cooling in low subsonic flows using LES. Work on jets in supersonic crossflow has been presented by Chenault et al. (1999) and Sriram & Mathew (2008) using statistical turbulence models. Kawai & Lele (2008) have performed LES of jet mixing in supersonic turbulent crossflow (without reaction) using high-order compact differencing schemes coupled with localized artificial diffusivity methods to properly capture shocks and contact surfaces. The present work focuses on transverse injection into subsonic crossflow and equilibrium chemistry to get insight into the physics, accompanying the rapid changes in the turbulence structure close to the injection slot.

FLOW CONFIGURATION

The study is a first step towards a detailed LES of ramjet combustion. It uses a simplified geometrical and physical configuration (Figure 1) to predict mixing and combustion processes during perpendicular injection into a subsonic turbulent channel flow and to test the feasibility of the LES approach. The flow entering the channel is fully-developed and has a bulk Mach number of 0.5 (based on bulk velocity and speed of sound at wall temperature), a bulk Reynolds number of 3000 (based on bulk mass flux, channel half width and viscosity at wall temperature) and a friction Reynolds number $Re_\tau = 198$. Walls are kept at constant temperature of 700 K. At a distance of 4 channel half widths downstream of the inlet, a plane jet injects a mixture of H_2/N_2 with mass fractions of 0.0169/0.9831 into the air stream with N_2/O_2 mass fractions of 0.77/0.23. The ratios of incoming mass and momentum flux rates of the injection channel (IC) to those of the main or combustion channel (CC) are $J_M = 0.043$ and $J_I = 0.62$, respectively. The ratio of channel half widths is, $h_1/h_2 = h_{CC}/h_{IC} = 16$.

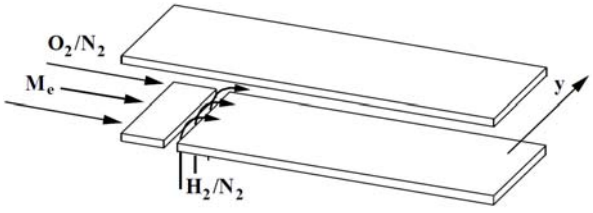

Figure 1. Schematic view of the statistically two-dimensional flow configuration (combustion channel, CC).

Infinitely fast reaction between hydrogen and oxygen is assumed and modelled by just one irreversible global reaction.

The bulk Reynolds and Mach numbers of the injected jet are 168 and 0.34, respectively. All these parameters are specified using global mass, momentum and energy balances in such a way that the mean flow speed in the combustion channel nowhere exceeds the local sonic speed. The instantaneous flow is periodic in the spanwise y-direction only. (x,z) denotes the main flow and its wall-normal direction, respectively.

Mathematical models

The working gas is a mixture of the ideal gases H_2, O_2, N_2 and H_2O, with varying species concentrations, $Y_\alpha = \rho_\alpha / \rho$, satisfying the equation of state

$$p = \rho R T, \tag{1}$$

in which T, p, ρ, R denote temperature, pressure, density and gas constant of the mixture. Specific heats of a gas component α, as well as their ratio $\gamma_\alpha = c_{p,\alpha}/c_{v,\alpha}$ depend on temperature. The following approximation is used (McBride *et al.* (1993)):

$$c_{p,\alpha} = \Re\left(a_{1,\alpha} + a_{2,\alpha}T + a_{3,\alpha}T^2 + a_{4,\alpha}T^3 + a_{5,\alpha}T^4\right)/W_\alpha \ , \tag{2}$$

which contains the universal gas constant $\Re$ and the molecular weights W_α. The coefficients $a_{i,\alpha}$ are taken from tables connecting two temperature ranges: 300 K to 1000 K and above 1000 K.

The dynamics of the flow follows the transport equations for mass, momentum, total energy and mixture fraction of a compressible reacting gas mixture in Cartesian coordinates,

$$\begin{aligned}
\frac{\partial \rho}{\partial t} &= -\frac{\partial \rho u_j}{\partial x_j}, \\
\frac{\partial \rho u_i}{\partial t} &= -\frac{\partial \rho u_j u_i}{\partial x_j} - \frac{\partial p}{\partial x_i} + \frac{\partial \tau_{ij}}{\partial x_j} + f_{Vi}, \\
\frac{\partial \rho E}{\partial t} &= -\frac{\partial \rho u_j E}{\partial x_j} - \frac{\partial p u_j}{\partial x_j} + \frac{\partial u_i \tau_{ij}}{\partial x_j} + u_i f_{Vi} \underbrace{- \sum_{\alpha=1}^{4} \Delta h^0_{f\alpha} \omega_\alpha}_{\omega} \\
&\quad \underbrace{+ \frac{\partial}{\partial x_j}\left(\lambda \frac{\partial T}{\partial x_j}\right) - \frac{\partial}{\partial x_j}\left(\rho \sum_{\alpha=1}^{4} h_{s,\alpha} Y_\alpha V_{\alpha,j}\right)}_{-\partial q_j/\partial x_j}, \\
\frac{\partial \rho \xi}{\partial t} &= -\frac{\partial \rho u_j \xi}{\partial x_j} + \frac{\partial}{\partial x_j}\left(\frac{\mu}{Sc}\frac{\partial \xi}{\partial x_j}\right).
\end{aligned} \tag{3}$$

In eq. (3), u_i, E, ξ, τ_{ij}, q_j, ω_α, $\Delta h^0_{f,\alpha}$ represent velocity components, total energy, mixture fraction, viscous stress and molecular heat flux components, mass production rate and standard enthalpy of formation of species α, respectively. f_{Vi} is a body force, needed to drive fully-developed channel flow in a precursor simulation that provides inflow conditions for the CC. While the heat release term ω is zero in the precursor simulation, f_{Vi} is zero in the CC. The mixture fraction ξ, $0 \le \xi \le 1$, is defined as

$$\xi = \frac{s_R Y_F - Y_O + Y_{O,o}}{s_R Y_{F,f} + Y_{O,o}} \quad with \quad s_R = \frac{\nu'_O W_O}{\nu'_F W_F}. \tag{4}$$

Y_F, Y_O denote the mass fractions of fuel and oxidiser, $Y_{F,f}$, $Y_{O,o}$ their respective mass fractions in the pure fuel and air streams, ν'_F, ν'_O, W_F, W_O their stoichiometric coefficients and molar masses. Inherent to the concept of a mixture fraction is the use of constant Schmidt numbers, $Sc = \mu/(\rho D) = 0.7$ for all species. D is the diffusion coefficient of any of the species in the mixture. The mass fractions are functions of the mixture fraction only and interrelated by the Burke-Schumann relations (Poinsot & Veynante 2005). Fuel (hydrogen H_2) and oxidizer (oxygen O_2) are assumed to react infinitely fast, according to the irreversible one-step reaction

$$2H_2 + O_2 \rightarrow 2H_2O. \tag{5}$$

The mass production rate in eq. (3) is given by

$$\omega_\alpha = -\chi \frac{d^2 Y_\alpha}{d\xi^2} \quad wherein \quad \chi = \rho D \left(\frac{\partial \xi}{\partial x_i}\frac{\partial \xi}{\partial x_i}\right) \tag{6}$$

is the scalar dissipation rate. ω_α vanishes except for the stoichiometric mixture fraction ξ_s,

$$\omega_\alpha = -\chi \frac{Y_{F,f}}{1-\xi_s}\delta(\xi - \xi_s) = -\chi \frac{d}{d\xi}\int \frac{Y_{F,f}}{1-\xi_s}\delta(\xi - \xi_s)d\xi. \tag{7}$$

The viscous stress in eq. (3) has the usual form

$$\tau_{ij} = 2\mu S_{ij} + (\mu_d - 2\mu/3) S_{kk}\delta_{ij}, \tag{8}$$

depending on the deformation tensor and the shear and bulk viscosities, μ, μ_d. Using Fick's law, we simplify the diffusion flux

$$\rho Y_\alpha V_{\alpha,j} \approx -\frac{\mu}{Sc}\frac{dY_\alpha}{d\xi}\frac{\partial \xi}{\partial x_j} \tag{9}$$

and hence the molecular heat flux q_j. The molecular transport coefficients μ, μ_d, λ for the gas mixture are computed efficiently using the programme EGLiB which is based on kinetic theory of gases (Ern & Giovangigli 1995). During the integration of the transport equations (3), the temperature T must be determined before each time step from the definition of the total energy E. This is done by solving a nonlinear 5th order equation in T iteratively, using the Brent algorithm (Press et al. 1992).

Semi-implicit LES approach. For an LES, the set of equations (3) has to be low-pass filtered in space. In order to avoid (explicit) modelling of each filtered nonlinear term, we perform explicit filtering of the equations (except for the heat

release term ω) at each time step with a composite filter, $(Q_N * G)^2$, as suggested by Mathew et al. (2003) and call it the implicit LES part. Q_N is, e.g. for the periodic direction, the approximate inverse of a 6th-order one-parametric Padé filter, G (Lele 1992). More details on explicit filtering applied to the case of a reacting jet in supersonic cross flow can be found in Schaupp & Friedrich (2010). The low-pass filtered term $\overline{\omega} = -\sum_1^4 \Delta h^0_{f,\alpha} \overline{\omega}_\alpha$ in the energy equation needs explicit modelling. We use a model which is the LES equivalent of the statistical model derived by Bilger (1980):

$$\overline{\omega}_{model} = 2Q_e \cdot \widetilde{\chi}_\xi(\xi_s) \cdot \widetilde{F}_\xi(\xi_s). \qquad (10)$$

An overbar denotes a quantity that is explicitly filtered with the above composite filter, and a tilde a corresponding density weighted quantity. In eq. (10) Q_e is an appropriate heat release parameter (Mahle et al. 2007) and $\widetilde{\chi}_\xi(\xi_s)$ the conditionally filtered scalar dissipation rate at the stoichiometric mixture fraction value ξ_s:

$$\widetilde{\chi}_\xi(\xi_s) = \int_0^\infty \zeta \widetilde{F}_{\zeta|\xi}(\zeta'|\xi = \xi') d\zeta'. \qquad (11)$$

$\widetilde{F}_\xi$ is the filtered density function (fdf) of the mixture fraction which is modeled by a beta function that involves the filtered mixture fraction (available from its filtered transport equation (3)) and the subgrid variance

$$\left(\xi^2\right)_{sg} = \overline{\xi^2} - \widetilde{\xi}^2, \qquad (2)$$

for which a gradient model is used.

Computational details

The low-pass filtered transport equations (3) are discretized in space using sixth-order compact central schemes (Lele 1992) and an explicit fourth order Runge-Kutta time-integration scheme (Kennedy et al. 1999).

At walls (of CC and IC) no-slip and impermeability conditions are imposed. Walls are isothermal and noncatalytic, which means that rates of reaction vanish. Thus, wall-normal diffusion fluxes disappear in wall grid points, e.g. the wall-normal flux of ξ. Inflow and outflow boundary conditions are based on a characteristic decomposition of the transport equations (see Sesterhenn (2001) and Mahle (2007)). The specification of outflow boundary conditions (especially for the pressure at the exit of the CC) is based on approximate integral balances of mass and momentum fluxes in the CC for the desired flow parameters.

A realistic LES of the jet in crossflow takes the flow in the injection channel into account. This only guarantees realistic injection conditions. In the present work the computational domain consists of three blocks. Block 1 represents the combustion channel, block 2 the injection channel and block 3 the inflow generator with fully developed non-reacting channel flow. Communication between the blocks is based on the MPI protocol and the decomposition of the transport equations in terms of acoustic, shear, entropy and mixture fraction (convective) waves. In order to avoid numerical instabilities which are generated at the sharp edges where IC and CC meet (when high-order schemes are used), the flow variables are filtered in a narrow vicinity of these edges applying explicit filters of Gaussian type.

Computation of derivatives across interfaces is achieved by means of ghost layers, using, wherever possible, the interior compact central finite difference scheme of sixth order. The grid is designed to perfectly match at interfaces in all spatial directions. The grid point distribution is uniform only in the spanwise y-direction. In wall-normal direction (z for the CC and x for the IC) the first point away from the wall has a distance of less than one wall unit, ν_w/u_τ. Relative grid-stretching is smooth and the variation of the point spacing is limited. The grid is strongly refined in main flow direction around the injection slot. The dimensions of the blocks are listed in wall-units in Table 1. Table 2 contains the number of grid points in each block.

Table 1.Dimensions of the three grid blocks in multiples of the wall units obtained in block 3.

	Block 1	Block 2	Block 3
L_x^+	2503, 4	417,1	3690,9
$L_y^+ = 4\pi h^+/3$	837,5	837,5	837,5
$L_z^+ = 2h^+$	399,8	25	399,8
h^+	199,9	12,5	199,9

Table 2.Number of grid points

	n_x	n_y	n_z
Block 1	512	64	128
Block 2	128	64	32
Block 3	160	64	128
Total number of points	$5.76 \cdot 10^6$		
Total number of CPUs	44		

Initial conditions for the CC are obtained from a separate RANS simulation with a (k, ε)-turbulence model, neglecting chemical reaction. Fluctuations taken from fully-developed channel flow (Block 3) are superimposed on the statistical steady state solution near the inlet of the CC.

During the LES performed on the SGI Altix 4700 supercomputer of the Bavarian Academy of Sciences, a total of about 650000 time steps have been computed. This includes about 450000 time steps before statistical evaluation starts. It does not include computational time needed to establish a proper inflow condition. The simulation used more than 2650 hours of wall clock time.

RESULTS

We start the discussion of results with instantaneous views of the jet in subsonic crossflow. The instantaneous flow

variables shown are $(Q_N * G)^2$ – filtered quantities, which, in order to simplify the notation, do not carry an overbar or a tilde. The overbar and the tilde are later needed to denote Reynolds and Favre averages, $\bar{a}, \tilde{a}$. The corresponding fluctuations are a', a'' , respectively.

Instantaneous flow variables

Figure 1 shows a snapshot of the local Mach number M (based on the velocity magnitude) as a carpet plot, together with two contour lines for M=0.3 and 0.6 in the mid-plane of the CC. Islands of low Mach number flow (M=0.3, white line) have left the recirculation zone downstream of the injection slot and are washed away. The injected, reacting jet accelerates the channel flow so that local mean Mach numbers reach maximum values close to 0.8.

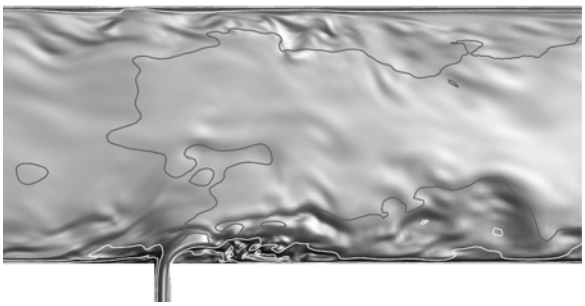

Figure 1. Local Mach number, based on magnitude of mean velocity.

Water vapour is the end product of the global reaction assumed. Its concentration is displayed in figure 2 in the same plane and at the same instant of time as chosen in figure 1. As the contour lines of the H_2O mass fraction with values of 0.01 and 0.05 show, chemical reaction takes place already on the upstream (windward) side of the jet where oxygen and hydrogen first get together. The figure also shows that water vapour occasionally enters the injection channel and gives rise to separation of the jet before it reaches the sharp upstream edge. This demonstrates the need to compute the flow in the injection channel simultaneously with that in the CC.

Figure 2. Mass fraction of water vapour. Black/white contour lines: $Y_{H_2O} = 0.01 / 0.05$

Projections of instantaneous velocity vectors into the vertical (y,z)-mid-plane of the IC provide an impression of the complexity of the turbulent mixing processes which take place in the mixing layer between fuel and air stream (see figure 3). Close to the lower channel plane, but still in the mid-plane of the jet, the velocity vectors are practically parallel which is due to the fact that the injected jet is still in a state of laminar flow there. At the upper wall the vectors indicate local streamwise vortices, induced by sweeps and ejections.

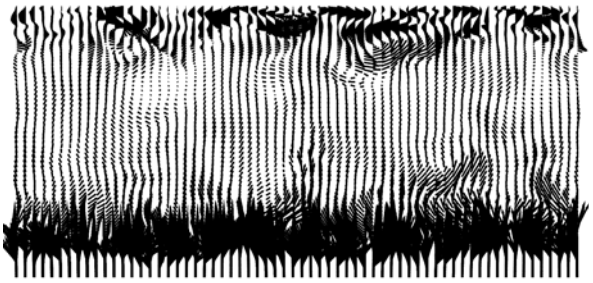

Figure 3. Velocity vectors projected into the vertical mid-plane of the injection channel (IC).

Statistically averaged flow variables

Figure 4 shows contours of the mean temperature, normalized with the constant wall temperature, T_w = 700 K. While the mean temperature of the incoming fully-developed flow exceeds the wall temperature by 5% in the core region, due to direct and turbulent dissipation, combustion in the mixing layer surrounding the jet raises it to values above 950 K at x/h_1 = 0 and above 1250 K at x/h_1 = 3. Combustion and mixing, however, are not the only mechanisms which control the temperature field. Other mechanisms are compression and expansion. Profiles of the mean pressure in figure 5 at different stations upstream and downstream of the slot (x/h_2 = 0), reveal compression/expansion effects of the mean pressure, compared to the wall pressure at the channel inlet. Taking into account that the mean pressure in fully-developed compressible channel flow varies only weakly normal to the

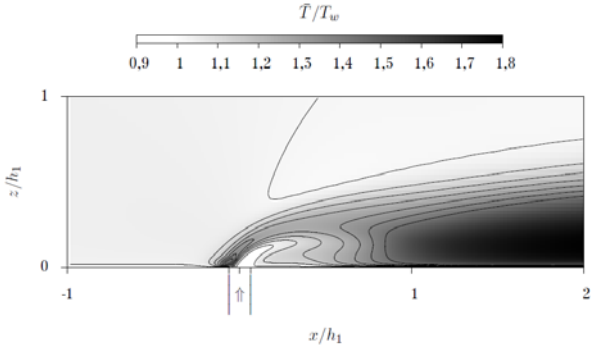

Figure 4. Mean temperature, normalized with its constant wall value (lower half of channel shown).

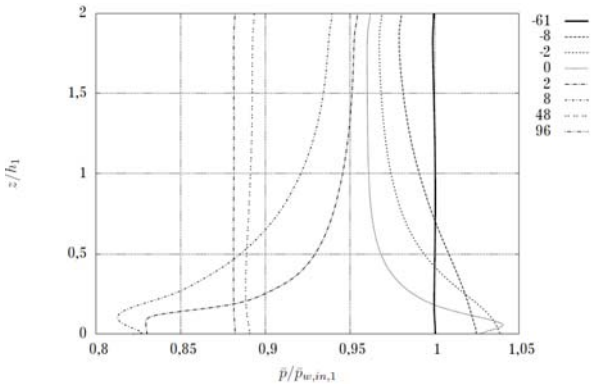

Figure 5. Profiles of mean pressure, normalized with its upstream wall value at different stations. Station $x/h_2 = 0$ corresponds to IC mid-plane.

wall, following the variation of the wall-normal Reynolds stress (Ghosh et al. 2010), the pressure profile at $x/h_2 = -61$ (solid line) does not show any variation on the chosen scale. The strong pressure variations observed at positions $x/h_2 = -8$, -2,0 are due to compression effects near the wall and due to expansion effects ($x/h_2 = 8,2$) downstream of the slot. Only 6 channel half widths h_1 (or 96 h_2) downstream of the IC mid-plane, the pressure has attained a practically constant value across the CC, which lies below its value at the inlet, as a result of flow acceleration. The described compression/ expansion effects are also reflected in the mean pressure distribution along both walls and the mid-plane in figure 6.

The mean pressure variations discussed entail effects of mean dilatation affecting the production of the Reynolds stress tensor. They enhance the Reynolds stresses when there is compression and dampen them during expansion. Besides production by mean dilatation there is, of course, production by mean shear. This mechanism provides the biggest contribution in regions where the jet is surrounded by mixing layers. We note that the streamwise Reynolds stress in figure 7, normalized with the wall shear stress at the inlet reaches values downstream of the jet which exceed the wall shear stress by a factor of 60 or more.

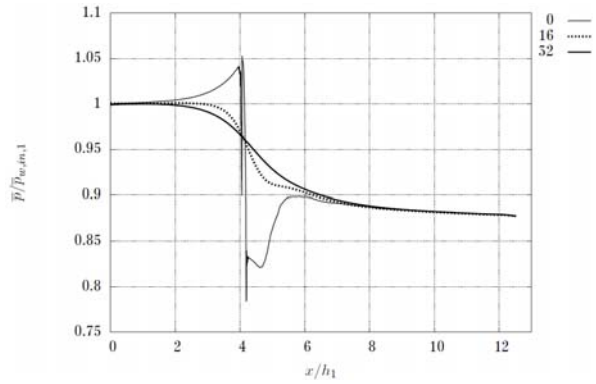

Figure 6. Streamwise distribution of mean pressure at the walls ($z/h_2 = 0, 32$) and in the mid-plane, $z/h_2 = 16$.

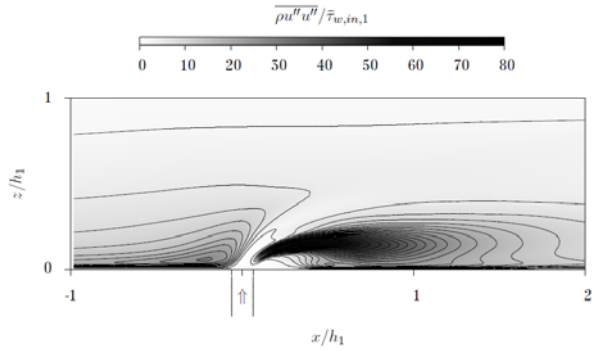

Figure 7. Streamwise Reynolds stress, normalized with upstream wall shear stress (lower half of channel shown).

The Reynolds shear stress in figure 8 shows dramatic changes in the neighbourhood of the injected jet. It even changes sign in

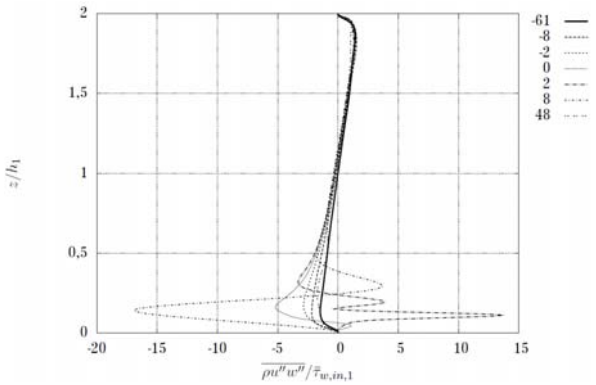

Figure 8. Reynolds shear stress, normalized with upstream wall shear stress.

different zones. The complexity of structural changes in the Reynolds stresses and their anisotropies becomes obvious when the second and third invariants of the corresponding anisotropy tensor for all points of the computational domain are plotted in one map. These points almost completely fill out the anisotropy invariant map (not shown). Hand in hand with these structural changes we observe dramatic changes in the production and redistribution terms for all stresses. As an example we show the pressure strain correlation for the streamwise stress balance, $\overline{p'\partial u'/\partial x}$, normalized with $\bar{\tau}^2_{w,in,1}/\bar{\mu}_{w,in,1}$ in figure 9. Changes in the pressure-strain correlations may partly be traced back to changes in the mean density (Foysi et al. 2004).

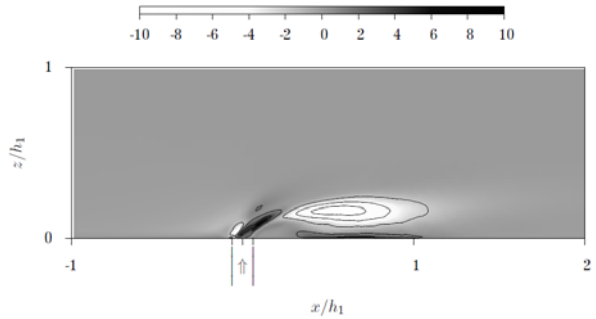

Figure 9. Normalized pressure-strain correlation of streamwise stress balance, $\overline{p'\partial u'/\partial x}$. (lower half of channel shown).

Conclusions

The complex thermo-fluid-dynamical flow problem of a plane reacting hydrogen jet which is injected perpendicularly into a fully turbulent, subsonic air flow is investigated using a semi-implicit LES technique. It is shown that the geometrically simple configuration can be treated with high-order compact numerical schemes, provided high-wavenumber perturbations which are generated at the sharp intersections between main and injection channel are locally controlled.

Snapshots of the flow field underline the necessity to include the flow in the injection channel during the LES, since it interacts with the crossflow. The mean flow shows a variety of flow phenomena such as flow separation upstream and downstream of the injection slot, deceleration and acceleration of the flow, mixing between air and fuel streams and finally chemical reaction. All these phenomena contribute to strong changes in the turbulence structure and make this flow configuration a challenging case for statistical turbulence prediction.

REFERENCES

Bilger, R.W., 1980. "Turbulent flows with nonpremixed reactants," in: P.A. Libby and F.A. Williams, eds., *Turbulent reacting flows*. Berlin, Springer Verlag, pp. 65-113.

Chenault, C. V., Beran, P. S., and Bowersox, R. D. W., 1999, "Numerical investigation of supersonic injection unsing a Reynolds-stress turbulence model," *AIAA Journal,* Vol. 37(10), pp. 1257-1269.

Denev, J. A., Fröhlich, J., and Bockhorn, H., 2009, „Large-eddy simulation of a swirling transverse jet into a crossflow with investigation of scalar transport," *Physics of Fluids,* Vol. 21, 015101.

Ern, A., and Giovangigli, V., 1995, „Fast and accurate multicomponent transport property evaluation," *J. Comp. Phys.,* Vol. 120, pp. 105-116.

Foysi, H., Sarkar, S., and Friedrich, R., 2004, "Compressibility effects and turbulence scalings in supersonic channel flow," *J. Fluid Mech.,* Vol. 509, pp. 207-216.

Ghosh, S., Foysi, H., and Friedrich, R., 2010, "Compressible turbulent channel and pipe flow: similarities and differences," *J. Fluid Mech.,* Vol. 648, pp. 155-181.

Jones, W. P., and Wille, M., 1996. "Large-eddy simulation of a plane jet in a crossflow," *Int. J. Heat Fluid Flow,* Vol. 17(3), pp. 296-306.

Kawai, S., and Lele, S. K., 2008, "Large-eddy simulation of jet mixing in a supersonic turbulent crossflow, " *CTR Annual Research Briefs,* pp. 139-151.

Kennedy, Ch. A., Carpenter, M. H., and Lewis, R. M. 1999, "Low-storage, explicit Runge-Kutta schemes for the compressible Navier-Stokes equation," *ICASE Technical Report* 99-22.

Lele, S. K., 1992 "Compact finite difference schemes with spectral-like resolution," *J. Comp. Phys.,* Vol. 103, pp. 16-42.

Mahle, I., 2007 "*Direct and large-eddy simulations of inert and reacting compressible turbulent shear layers*", Ph.D. thesis, Technische Universität München.

Mahle, I., Sesterhenn, J., and Friedrich, R., 2007. "Turbulent mixing in temporal compressible shear layers involving detailed diffusion processes," *J. Turbulence*, Vol. 8(1), 1468-5248.

Margason, R. J., 1993, "Fifty years of jet in crossflow research", *AGARD CP 534*, pp. 1-1 to 1-41.

Mathew, J., Lechner, R., Foysi, H., Sesterhenn, J., and Friedrich, R., 2003, „An explicit filtering method for large-eddy simulation of compressible flows", *Physics of Fluids,* Vol. 15, pp. 2279-2289.

McBride, J.B. and Gordon, S. and Reno, M., 1993, "Coefficients for Calculating Thermodynamic and Transport Properties of Individual Species", NASA Technical Memorandum 4513

Muppudi, S., and Mahesh, K., 2007, "Direct numerical simulation of round turbulent jets in crossflow," *J. Fluid Mech.,* Vol. 574, pp. 59-84.

Poinsot, T., and Lele, S. K., 1992 "Boundary conditions for direct simulations of compressible viscous flows," *J. Comp. Physics,* Vol. 101, pp. 104-129.

Poinsot, T., and Veynante, D., 2005, *Theoretical and Numerical Combustion.* 2nd ed. Flourtown, PA: R.T. Edwards.

Press, W.H. et al., 1992, *Numerical recipes in Fortran 77: the art of scientific computing.* 2nd ed., Cambridge Univ. Press.

Renze, P. and Meinke, M. and Schröder, W., 2008, „Large-eddy simulation of film cooling flows at density gradients," *Int. J. Heat Fluid Flow,* Vol. 29, No. 1, pp. 18-34

Schaupp, Ch., and Friedrich, R., 2010, „Large-eddy simulation of a plane reacting jet transversely injected into supersonic turbulent channel flow," *Int. J. Comp. Fluid Dyn.,* Vol. 24, No. 10, pp. 407-433.

Sesterhenn, J., 2001. "A characteristic-type formulation of the Navier-Stokes equations for high-order upwind schemes," *Comp. Fluids* Vol. 30, No. 1, pp. 37-67.

Sriram, A. T., and Mathew, J., 2008, "Numerical simulation of transverse injection of circular jets into turbulent supersonic streams,"*Propulsion and Power,* Vol.24, pp. 45-54.

Wegner, B., Huai, Y., and Sadiki, A., 2004, "Comparative study of turbulent mixind in jet in cross-flow configuration using LES," *Int. J. Heat Fluid Flow,* Vol. 25, pp. 767-7